Model for aging in HCl-protonated polyaniline: Structure, conductivity, and composition studies

A. Wolter, P. Rannou, and J. P. Travers*
Laboratoire de Physique des Métaux Synthétiques UMR 5819 (CEA-CNRS-UJF), Département de Recherche Fondamentale sur la Matière Condensée, CEA-Grenoble, 38054 Grenoble, Cedex 9, France

B. Gilles and D. Djurado*
Laboratoire de Spectrométrie Physique UMR 5588 (CNRS-UJF), Université Joseph Fourier Grenoble I, Boîte Postale 87, 38402 St. Martin d'Hères, Cedex, France

(Received 3 March 1998)

We present a comprehensive study of the aging process in HCl-doped polyaniline exposed to air. A complete set of measurements was carried out on three series of samples stemmed from the same preparation batch, and aged at 100, 120, and 140 °C for times up to one month. All the samples were studied by x-ray-diffraction and conductivity measurements in the 4.2–300-K temperature range, and by thermogravimetric and elemental analyses. The analysis of the x-ray data points out the heterogeneous character of the aging process. An amorphous phase (*F* phase) is shown which grows at the expense, first, of the amorphous emeraldine salt (ES-I) phase and, then, of the crystalline ES-I phase. We show that whatever the aging time, the conductivity can be described in terms of hopping between conducting grains separated by insulating barriers leading to $\sigma(T)=\sigma_0\cdot\exp[-(T_0/T)^{1/2}]$. The thermogravimetric and elemental analyses data give evidence of several chemical transformations: (i) a slight dedoping due to HCl evolution, (ii) an oxidation of the polymer backbone, and (iii) a chlorination of the rings. We propose a picture for the aging mechanism that accounts for the whole set of data with a particular emphasis on the quantitative evolution of both the *F* phase volume content and the hopping conductivity parameter T_0. The pristine conducting grains would consist of a crystalline core of emeraldine salt (ES-I) surrounded by ''paracrystalline'' and amorphous ES-I shells. The aging phenomena would then appear as a nibbling mechanism of conducting grains due to a progressive transformation of the doped polyaniline into the *F* phase, starting from the grain periphery, i.e., the most disordered parts of the material, toward the crystalline cores. Moreover, this model allows one to reproduce quantitatively the kinetics of the conductivity decrease at a given temperature. [S0163-1829(98)05936-0]

I. INTRODUCTION

Considerable attention from scientists and engineers has been paid to intrinsically conducting polymers such as polypyrrole, polythiophene, and polyaniline because of their high conductivity and their rather good stability. Among them, polyaniline, which is very cheap, and exhibits many interesting properties related to its easy reversible protonation, appears as one of the most promising for applications.

A number of studies have been devoted to the thermal stability of polyaniline,[1–14] mainly by means of thermogravimetric analyses. A few of them reported data from other characterization techniques such as elemental analysis,[1,2,9,11] differential scanning calorimetry,[1,5] x-ray photoelectron spectroscopy (XPS),[2,3,7,9,10] infrared spectroscopy,[1,2,4–7] UV-visible spectroscopy,[4,7] and conductivity measurements.[1,2,4,8,10–14] The conductivity was clearly shown to decrease with time,[1,2,4,10,13,14] with a rate depending on the nature of the dopant (counterion) as well on the morphology of the material. From the chemical point of view, several processes are invoked to take place in HCl-doped polyaniline upon heating: loss of dopant, chlorination of the aniline rings, oxidation of the chains due to oxygen, hydrolysis, and cross-linking. But even though conductivity is one of the leading properties of conducting polymers and of polyaniline (Pani) for applications, almost no systematic study has been carried out to quantify the long-term evolution of the conductivity and obtain a better understanding of the relation between the creation of chemical defects during degradation and the decrease of the conductivity.

As a matter of fact, such studies, which consist of following the evolution of the conduction mechanism as a function of aging, have appeared to be very fruitful in the case of polypyrrole[15–17] and poly (*p*-phenylenevinylene).[18] In particular, they have led (in the case of polypyrrole) to an unambiguous discrimination between the various conduction models proposed for polypyrrole. They clearly indicated that electronic conduction proceeds through hopping between conducting grains separated by insulating barriers. As far as aging is concerned, it appears as a sort of nibbling of the conducting grains to the benefit of the insulating barriers. Does the same picture apply in the case of polyaniline? A preliminary study carried out on highly conducting camphor sulfonic acid protonated polyaniline (Pani-CSA) concluded in favor of a similar type of aging mechanism.[14] In the case of Pani-HCl, for which several studies have pointed out the existence of isolated conducting islands,[19] this question takes a particular meaning.

In this paper, we present a comprehensive study of the aging mechanism in Pani-HCl under ambient air atmosphere.

It is based on x-ray-diffraction measurements, conductivity measurements as a function of temperature, and thermogravimetric and elemental analyses on a series of samples coming from the same batch of pristine material and then aged at a fixed temperature for different times ranging from zero to ten days. This is, to our knowledge, the first x-ray diffraction and detailed study of the transport properties devoted to the aging of polyaniline. We show here how results of these two joint studies lead to a reliable picture for the aging mechanism in Pani-HCl. Aging appears as an inhomogeneous process. All the data can be interpreted in terms of conducting grains separated by insulating barriers. Assuming, in the framework of this picture, that the aging process starts in the most disordered parts of the unaged material, and then extends toward the crystallized inner part of the grain in a diffusivelike manner, we succeed in quantitatively accounting for both x-ray and conductivity data with only a few parameters. From elemental and thermogravimetric analyses, it appears that the loss of dopant is not the leading process of aging. We suggest that oxidation of the chains by air oxygen works as the activating factor for subsequent chlorination of aniline rings.

This paper is organized as follows. Experimental details about samples and measurements are given in Sec. II. The chemical mechanisms of aging are discussed from elemental and thermogravimetric analyses in Sec. III. Section IV is devoted to a thorough analysis of the x-ray data. The data we obtained for the temperature dependence of the conductivity are reported and analyzed in Sec. V. Finally, a discussion of the results and their interpretation in the framework of the conducting grains picture are presented in Sec. VI.

II. EXPERIMENTAL DETAILS

A. Synthesis, preparation, and aging procedure of samples

Emeraldine hydrochloride (Pani-HCl) was synthesized by a conventional method developed by Mac Diarmid *et al.*[20] Typically for synthesis conducted at -5 °C, the polymerization was stopped after 90 min, and the reaction medium was filtered.[21] A green-blue precipitate was collected and washed with copious amounts of 1 M HCl until the filtrate became colorless. Pani-HCl was then dried overnight at 50 °C under nitrogen flushing at a constant pressure of 25 mbar. This as-synthesized emeraldine hydrochloride was deprotonated by stirring in 0.1 M ammonium hydroxide for 72 h. The emeraldine base (EB) obtained after this dedoping procedure was filtered and washed several times with water. It was dried to constant weight under N_2 at 25 °C ($\approx$24 h at 25 mbar). The EB was converted into Pani-HCl by protonation in a 1 M HCl aqueous solution for 24 h. This reprotonated Pani-HCl was then dried to constant weight under N_2 at 25 °C ($\approx$24 h at 25 mbar), and used in the following aging procedure. Pani-HCl powders were aged under ambient air at three different temperatures: 100, 120, and 140 °C. Typically, for a given temperature, seven samples of about 100 mg of Pani-HCl originating from the same batch were placed in an oven. They were removed after different aging times t_a ranging from 52 min to ten days (see Tables I and II). The choice of the different aging times t_a was adapted to the progressive slowdown of the conductivity decay.

B. Thermogravimetric and elemental analyses

Thermogravimetric analysis (TGA) was performed on a Setaram TGDTA92 system. The analyses were carried out using 15 mg of powdered non-aged Pani-HCl and EB samples under a nitrogen or air flushing at a heating rate of 10 °C/min. Sample residual weight (TG curves) and its derivatives (DTG curves) versus temperature were automatically generated by the Setaram system. Elemental analyses were performed in Laboratoire Central d'Analyses from Centre National de la Recherche Scientifique in Vernaison (France).

C. X-ray analysis

All x-ray profiles have been recorded in the same experimental conditions. The powdered sample was placed in a capillary glass tube of 0.5 mm in diameter. The $K\alpha$ radiation of copper was produced by a 1200-W x-ray tube (Seifert), then the $K\alpha 1$ radiation was selected by using a curved crystalline blade of Ge(111) as a monochromator mounted in an asymmetric Johansson configuration (Huber). The two-circle goniometer we used was based on a PW 1835 one from Philips. The diffraction experiments were done by using the so-called Debye-Scherrer geometry, in which the x-ray beam was focusing on the detector window after passing through the sample. The detector was a linear multichannel position-sensitive one from Raytech. It was constituted of 1024 channels placed every 0.02° in 2θ. When recording an elementary 2θ step scan, we used 800 channels as an aperture of the detector window, a physical step of 0.06° in 2θ and a step duration of 4 s. Such a scan was then repeated 10–18 times for each sample and the sum of all these recordings gave a profile which was normalized in order to be compared with the others. The diffuse background due to the air and the glassy tube was periodically evaluated and subtracted from the diffractograms in order to keep only the signal scattered from the sample itself.

D. Conductivity measurements

Conductivity measurements have been performed on pellets obtained from powder by applying a 9-tons/cm^2 pressure for 3 min. Absolute values of the room-temperature conductivity have been obtained by the four-point method.[22] Typical values of the spacing between the aligned point contacts, thickness, and diameter of the circular pellets were 1, 0.8, and 8 mm, respectively. Conductivity values were deduced under the assumption of a semi-infinite medium, and corrected for a finite sample size. The temperature dependence of the conductivity was also measured by a four-contact method. To establish a good electrical contact, four flat gold pads were pressed on the sample. The probe head was placed in a continuous-flow helium cryostat permitting operation between 5 and 300 K. The sample temperature was measured by a rhodium iron resistance thermometer. The accuracy of the temperature measurement is better than 1 K at room temperature, and better than 50 mK at 5 K. To eliminate voltage offsets, the conductivity was always measured for both polarities of the current. Furthermore, linearity was checked for each point. Current was supplied by a Keithley Model 220 current source, the potential of the two voltage contacts was measured independently by two electrometers (Keithley Model 6512) using the guard technique.

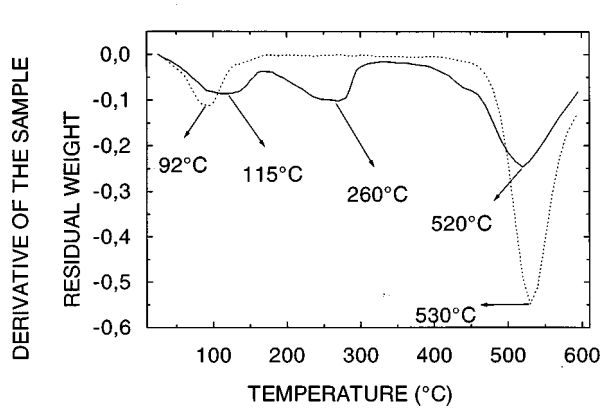

FIG. 1. Thermogravimetric analysis of the emeraldine base EB (dotted line) and Pani-HCl (solid line) under nitrogen atmosphere. The curves represent the derivative of the sample residual weight (DTG curves).

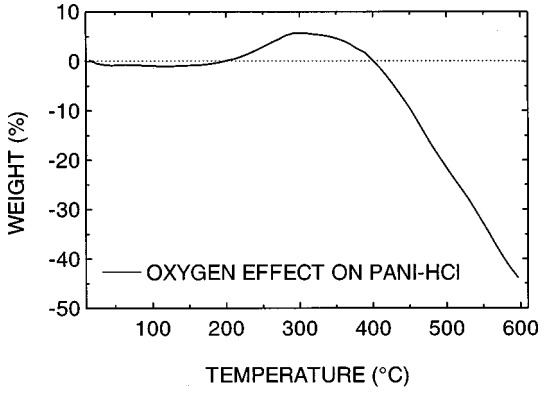

FIG. 2. Thermogravimetric analysis of Pani-HCl: difference of behavior under air and under nitrogen. The curve is obtained from the difference of the sample residual weight curves (TG curves) obtained in both conditions.

III. THERMOGRAVIMETRIC AND ELEMENTAL ANALYSES

The DTG curves of the EB and Pani-HCl under nitrogen are shown in Fig. 1. The thermogram of the EB shows typical two-step weight loss behavior, as can be deduced from the two maxima of the DTG curve.[23,24] The first one extends from room temperature to 150 °C. It can be attributed to a desorption of water molecules physically sorbed in the polymer matrix.[25,26] The second weight loss starts typically around 425 °C. This has previously been attributed to thermal decomposition of the polyaniline backbone structure.[23] The thermogram of Pani-HCl shows a typical three-step weight-loss behavior also observed previously by other authors.[1] The first weight loss corresponds to a maximum at 115 °C. The second weight loss occurs between 170 and 320 °C, and is followed by a final step starting at 420 °C.

In order to study the chemical change, the chemical composition of unaged and aged samples was examined by elemental analyses. The mass fraction of oxygen was derived in order to complement the sum of carbon, hydrogen, nitrogen, and chlorine fractions to 100%. The data are reported in Table I. The most striking result is the very low decrease of the chlorine concentration upon aging in air. Less than 10% of the total mass of chlorine has disappeared after ten days at 140 °C probably through gaseous HCl evolution. This result is in agreement with that of Ref. 2. It rules out the hypothesis of the loss of dopant as the main aging mechanism for Pani-HCl in air. Redoping with HCl after aging in nitrogen leads only to a very partial recovering of the conductivity.[1] Nevertheless a slight deprotonation exists, as confirmed by DTG. The difference in shape between the first maximum for the EB and Pani-HCl suggests that, in the case of Pani-HCl, not only a desorption of water is observed. We propose that below 160 °C, Pani-HCl loses mainly water and a small proportion of gaseous HCl originating from a slight deprotonation process. But most of the HCl loss should then occur during the second weight loss together with water molecules which are more strongly bonded to the polymer in Pani-HCl than in the EB. The third step consists mainly of a thermal decomposition of the polyaniline backbone.

Under air, the second weight loss of Pani-HCl seems to disappear. This suggests that an oxidation process takes place in the same temperature range, and tends to compensate for the weight loss previously observed under nitrogen. Therefore, to reveal the effect of oxygen on the thermal stability of Pani-HCl, air, and nitrogen thermograms were subtracted. The resulting curve is shown in Fig. 2. An additional gain of mass under oxygen occurs between 150 and 300 °C, followed by a pronounced loss above 380 °C. This mass uptake can be attributed to an oxidation process. Then the residual modified polymer burned under oxygen. The existence of such an oxidation process is also clearly supported by elemental analyses. Upon heating in air, one can observe a regular and large decrease of the H/C ratio as a function of aging time, while the O/C ratio is first decreasing and then slightly increasing at long aging times. Since only a few parts of HCl have quitted the material, most of the H/C ratio

TABLE I. Elemental analysis of Pani-HCl as a function of the aging time at 140 °C. Chemical compositions are normalized with respect to the carbon one, which is maintained constant at 6.00.

		Elemental analysis					Chemical composition				
	t_a (min)	C (%)	H (%)	N (%)	Cl (%)	O (%)	C	H	N	Cl	O
0	0	58.90	5.31	11.22	11.56	13.00	6.00	6.44	0.98	0.40	0.99
1	52	60.67	4.72	11.59	12.02	11.00	6.00	5.93	0.99	0.40	0.82
2	181	61.29	4.47	11.72	11.87	10.64	6.00	5.21	0.98	0.39	0.78
3	1398	62.37	4.10	12.16	11.78	9.59	6.00	4.70	1.00	0.38	0.69
4	4298	62.04	3.84	12.24	11.59	10.29	6.00	4.42	1.01	0.38	0.75
5	15 798	61.40	3.52	12.31	11.00	11.70	6.00	4.10	1.03	0.36	0.86

decrease can be attributed to an evolution of water molecules. This evolution leads to a reduction of the O/C ratio, as observed experimentally at short aging times. Therefore a concomitant and progressive oxidation of the polymer has to be invoked to explain first the stabilization of the O/C ratio and, then, its further increase. This point is evidenced when trying to account for the raw data of Table I using chemical formulas. Considering the unaged sample, a very good agreement is obtained with $(C_6H_{4.5}N_1)(HCl)_{0.4}(H_2O)_{1.0}$. Conversely, for the sample aged for ten days at 140 °C, the data can only be accounted for by $(C_6H_{3.64}N_1O_{0.86})(HCl)_{0.36}$. This formula is consistent only if it is considered that the chains have been oxidized. Only assumptions can be made concerning the nature of this process. Carbonylation of rings is very likely, but an oxygen-catalyzed hydrolysis followed by the formation of quinone terminal groups cannot be ruled out. Both processes should result in a decrease of the conjugation length and hence of the conductivity.

Then, remains the question of the nature of the chlorine species. In the unaged sample, most of them exist as Cl^- counterions, ionically bonded to the chains and therefore participating to the doped state of the system. However, a small proportion of covalently bonded chlorine species has been shown to exist by XPS.[2,27] Upon aging in the presence of air, at 150 °C for 100 h, the same authors[2] concluded from XPS studies that all the chlorine atoms were covalently bonded. Since upon aging in vacuum they did not observe this effect, they suggested that in presence of air, chloride ions are consumed by chlorination of rings. Such a mechanism would of course lead to a dedoping of the polymer and to a loss of conductivity. Moreover, one would expect some changes in the structure. Actually, the material, which is originally composed of doped Pani chains together with intercalated Cl^- counterions, would be finally only made of dedoped substituted Pani chains.

IV. X-RAY SCATTERING ANALYSIS

A. Decomposition of the diffraction patterns

1. Global evolution of x-ray profiles as a function of the aging time

The x-ray profile of the unaged sample is shown in Fig. 3(a). The structure can be identified as emeraldine salt ES-I as previously denominated by Pouget *et al.*[28] As the aging time is increasing, the amorphous background of x-ray profiles becomes larger and larger especially around $2\theta \approx 20°$ as can be seen in Fig. 3. For a ten-day aging time at 140 °C, the Bragg peaks disappeared; the material turned completely amorphous. This has been the only case for which such a state was fully reached. The evolution of the x-ray profiles during aging is strongly reminiscent of the evolution as a function of the doping level observed by Pouget *et al.*[28] In particular, the amorphous phase we obtained after ten days at 140 °C looks like the fully dedoped phase-denominated emeraldine base EB-I phase by Pouget *et al.*[28] Thus it can be said that the prominent phenomenon occurring as a function of aging time is the progressive evolution of the structure from ES-I phase toward an ''EB-I-like'' phase which will be denominated ''*F* phase'' in the following. This latter cannot

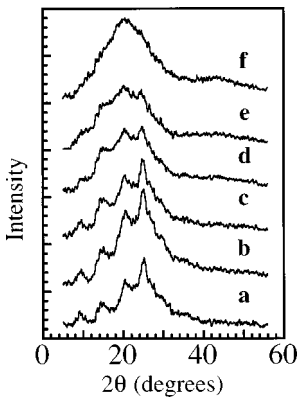

FIG. 3. Evolution of the x-ray profiles of samples heated at 140 °C as a function of the aging time t_a with (a) $t_a = 0$, (b) $t_a = 52$ min, (c) $t_a = 181$ min, (d) $t_a = 1$ day, (e) $t_a = 3$ days, and (f) $t_a = 10$ days. Curves are offset for more clarity.

be completely assimilated to EB-I since, according to elemental analysis results, 90% of Cl is still present within the sample even the most aged ones.

2. Evolution of the diffuse background as a function of the aging time

Since, the crystalline part of the x-ray profiles can be unambiguously attributed to the doped ES-I phase; it is possible to consider separately the evolution of the diffuse background of the profiles. Figure 4 shows the evolution of the diffuse background at 140 °C for different aging times. At this stage of the analysis, the profiles were obtained by interpolation in between 12 points taken at the minima between the Bragg peaks. From the figure, it can be seen that a broad component centered at $2\theta = 20.3°$ is progressively increasing, as mentioned before. For the shortest aging times, almost the whole diffuse background can be attributed to the disordered parts of the doped ES-I phase. It can be described with a first intense contribution at $2\theta = 25.5°$ and a broader one at about 23°. For the fitting procedure, the diffuse background is described by a superposition of the different contributions coming from *F* and ES-I phases. Thereby, weight factors *a* and *b* assigned to the two components vary with aging time:

$$I_{\text{amorphous}} = a(t_a) I^F + b(t_a) I^{\text{ES-I}}_{\text{amorphous}}. \tag{1}$$

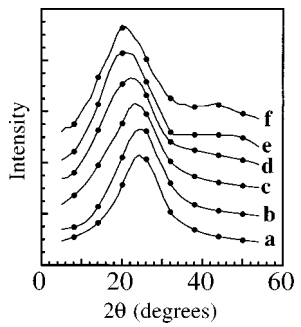

FIG. 4. Diffuse background of x-ray profiles of samples heated at 140 °C as a function of the aging time t_a with (a) $t_a = 0$, (b) $t_a = 52$ min, (c) $t_a = 181$ min, (d) $t_a = 1$ day, (e) $t_a = 3$ days, and (f) $t_a = 10$ days. Curves are offset for more clarity.

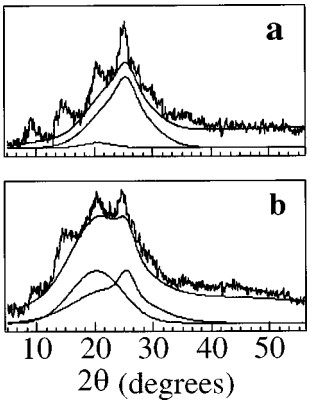

FIG. 5. An example of results obtained after fitting the diffuse background with three Gaussian contributions (see text): (a) sample heated at 140 °C for $t_a=0$ and (b) sample heated at 140 °C for $t_a=1$ day. All the components and their sum are shown and compared with the experimental profile.

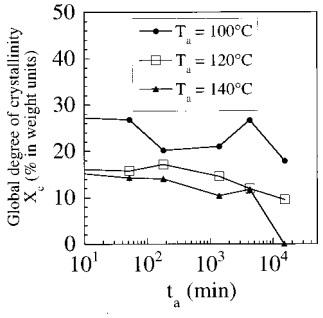

FIG. 6. Global degree of crystallinity as a function of the aging time (on a log scale).

More precisely, I^F is modeled by one Gaussian line centered at $2\theta=20.3°$. The other contribution coming from phase F is neglected, i.e., the broadband at 43.3° only visible for the very aged samples. The amorphous part of ES-I is modeled by two Gaussian lines. The first one is centered at 25.5° and has a width which is constrained not to be larger than 4°. The second around $2\theta=23°$ is allowed to be broader. An additional degree of freedom is introduced in this two-phase F/ES-I description by letting the weight factors of the two lines assigned to the amorphous part of ES-I to be freely fitted. In other words, the composition of the amorphous part of ES-I may change during aging. For more simplicity, the first contribution will be designated as the ''paracrystalline'' one, to be distinguished from the second one we still label as the ''amorphous'' one. The respective evolutions of these two contributions, which are the signatures of two different types of disorder, have no reason to be simply correlated.

In summary, the diffuse background of each recorded x-ray profile has been described as the sum of three Gaussian components:

$$I_{\text{amorphous}}(t_a)=\sum_{i=1}^{3} a_i e^{4\ln 2(2\theta-2\theta_i)^2/l_i^2}. \tag{2}$$

Moreover, at the highest diffraction angles, the diffracted intensity tends to a nonzero constant value due to the incoherent scattering. This effect can be accounted for by adding a second order polynomial function to the diffuse background:[29]

$$I_{\text{incoherent}}=b_1+b_2(2\theta)+b_3(2\theta)^2. \tag{3}$$

TABLE II. Evolution of the composition and conductivity during the aging process. Concentration of F phase C_F, s/d calculated from fit of Eq. (10), room-temperature conductivity σ_{RT}, exponent γ, and characteristic temperature T_0 for different aging temperatures T_a and aging times t_a. T_0 results are from fits of Eq. (6), for which γ has been fixed to $\frac{1}{2}$.

T_a (°C)	t_a (min)	C_F	s/d	σ_{RT} (S cm^{-1})	γ	T_0 (K)
140	0	0.0293		5.32×10^{-1}	0.33	10 620
140	52	0.0826	0.027	5.21×10^{-2}	0.36	16 270
140	181	0.145	0.052	5.78×10^{-3}	0.38	21 190
140	1398	0.398	0.16		0.39	67 330
140	4298	0.677	0.32		0.7	162 500
140	15 798	1.0	0.82			
120	0	0.0072		1.23×10^{0}	0.35	5117
120	52	0.0315	0.019	2.65×10^{-1}	0.37	12 950
120	181	0.103	0.036	7.53×10^{-2}	0.34	13 540
120	1398	0.344	0.11		0.38	25 730
120	4298	0.433	0.20	6.93×10^{-5}	0.37	39 850
120	15 798	0.810	0.47			
100	52	0.0547	0.0061	8.30×10^{-1}	0.30	5428
100	181	0.160	0.011	6.19×10^{-1}	0.32	6078
100	518		0.019	2.50×10^{-1}	0.34	8833
100	1398	0.113	0.032	7.34×10^{-2}	0.36	12 050
100	4298	0.151	0.058	1.91×10^{-2}	0.40	14 880
100	15 798	0.401	0.12	2.15×10^{-3}	0.43	21 420

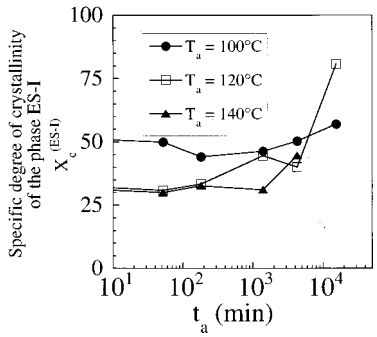

FIG. 7. Degree of crystallinity specific of the ES-I phase as a function of the aging time (on a log scale).

The fitting procedure was then carried out with the following conditions: $2\theta_1 = 20.3°$, $2\theta_2 = 25.5°$, $22° \leqslant 2\theta_3 \leqslant 25°$, $2° \leqslant l_2 \leqslant 4°$, $3° \leqslant l_1 \leqslant 11°$ and $2.5° \leqslant l_3 \leqslant 6°$.

Convergence was obtained in all cases. An uncertainty of 12% has been evaluated for the intensities of the three lines, while 10% was the estimated error on the widths of lines. By subtracting this diffuse background from the total diffraction pattern, the crystalline part is obtained, and then the degree of crystallinity can be evaluated more precisely. All the profiles of the 18 studied samples have been analyzed in such a way, only one example is shown by Fig. 5 in order to illustrate the quality of fits.

B. Structural changes induced by aging

1. Evolution of the crystalline structure as a function of the aging time

The degree of crystallinity per weight units has been estimated using the following formula, which is the simplest one that can be deduced from earlier work done by Ruland:[30]

$$X_c = \frac{\int I_{\text{cryst}}(2\theta)d(2\theta)}{\int I_{\text{cryst}}(2\theta)d(2\theta) + \int I_{\text{amorphous}}(2\theta)d(2\theta)}. \quad (4)$$

From Fig. 6, it can be clearly seen that X_c does not change very much upon aging. This is in sharp contrast to the room-temperature conductivity, which even for the lowest aging temperature $T_a = 100\,°\text{C}$ decreases by about three orders of magnitude (see Table II). This result indicates that crystallinity and conductivity are not simply correlated.

A careful analysis of the widths of peaks shows that they do not vary in any significant amount. In particular, no noticeable broadening is observed, proving that the loss of crystallinity is mainly due to a progressive disappearance of crystalline domains in number rather than their progressive diminution in size. In some sense, this is the exact reverse situation than that reported by other authors who studied the crystallization of polyaniline under stretching.[29] The reason why some of the crystallites are surviving longer than others to the degradation is not quite clear. We believe that the most stable ones are those which are the most crystalline and which are surrounded by the largest ''shells'' constituted of ''paracrystalline'' doped ES-I domains.

2. Specific degree of crystallinity of the ES-I phase

Considering the ES-I phase itself, all the results previously described suggest that it progressively disappears, while its crystalline part is not dramatically affected. In other words, it is possible to define a specific degree of crystallinity of this phase as follows:

$$X_c^{\text{ES-I}} = \frac{\int {}^{\text{ES-I}}_{\text{cryst}}(2\theta)d(2\theta)}{\int I^{\text{ES-I}}_{\text{cryst}_s}(2\theta)d(2\theta) + \int I^{\text{ES-I}}_{\text{amorphous}}(2\theta)d(2\theta)}. \quad (5)$$

As shown in Fig. 7, it can be seen that this quantity slightly increases with aging. That proves that the chemical reactions induced by aging proceed first in the more disordered regions surrounding the crystallites and that the crystallites themselves are destroyed only at the very end of the aging process.

3. Growth of the F phase as a function of the aging time

Knowing the respective contributions of *F*, amorphous ES-I, and crystalline ES-I phases, the proportion in weight units of the *F* phase contained in the sample is easily calculated. As expected, this proportion is increasing as a function of the aging time (see Table II). The most interesting point is how the *F* phase grows up. Considering the simultaneous evolution of the ES-I phase, it appears that the initial regime actually corresponds to a progressive disappearance of the diffuse line centered at 25.5° in 2θ, and to a lesser extent of the broader line centered at 23° in 2θ. In other words, the disordered, ''paracrystalline'', and amorphous components of the ES-I phase are first affected. That means that the chemical reactions occur more easily in those disordered regions because it is likely easier for the different involved chemical species to diffuse in these regions than in the more densely packed crystalline parts of the sample.

In summary, from x-ray analysis, it appears that the aging process in a first step affects the most disordered parts of the starting fully doped sample. In a second step, the microstructure of the sample can be seen as small doped crystallites embedded in an amorphous insulating matrix. At the last stage, the crystallites themselves disappear. For long aging times, the material is only composed of the *F* phase and its conductivity has become very low, as will be shown in Sec. V. This *F* phase would be characterized by the existence of oxidized and chlorinated Pani chains, as discussed in Sec. V B 2, and therefore, it is not so surprising that the *F* phase is insulating. The whole process is clearly inhomogeneous in nature and that indirectly suggests the starting microstructure of the ES-I system is constituted of crystallites, which are separated by disordered shells. As aging first concerns the most disordered regions between the crystallites, after a while, the sample consists of an assembly of conducting grains including the crystallites and the doped part of their disordered shells, separated by insulating shells of amorphous phase *F*. With the exception of the $[F]/[\text{ES-I}]$ ratio, the structural parameters are only a few changed by the aging process. Thereby, $[F]/[\text{ES-I}]$ is the only structural parameter, that can be correlated with the conductivity. In Secs. V B 2 and VI, the idea that the $[F]/[\text{ES-I}]$ ratio is related to

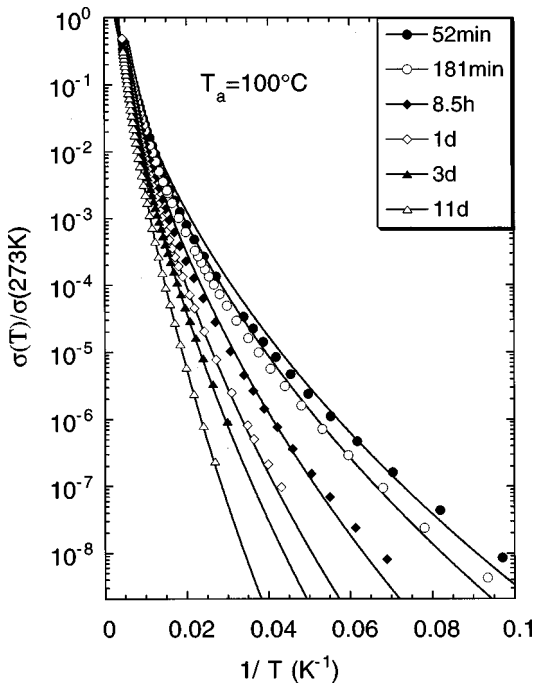

FIG. 8. Temperature dependence of the normalized conductivity $\sigma(T)/\sigma(273\ \mathrm{K})$ of Pani-HCl aged at 100 °C. Solid lines are fits of Eq. (6) with $\gamma=\frac{1}{2}$.

the ratio of the diameter of conducting grains to the thickness of the surrounding insulating barriers is the starting point for modeling the kinetics of degradation and the evolution of the conductivity with aging.

V. ELECTRICAL CONDUCTIVITY

Influence of water

Since polyaniline is known to absorb important quantities of water, which in turn changes the conductivity,[31] the proper initial conditions have to be chosen. Our study was performed with samples that were systematically in equilibrium with ambient air for a long time. To limit the loss of water during cooling down, samples were inserted in the cryostat maintained at ≈ -10 °C. Nevertheless the influence of the water content on the conductivity has been checked for extreme conditions. We compared the temperature dependence of the conductivity, i.e., of the parameters σ_0, T_0, and γ defined below in Eq. (6) for the same nonaged sample before and after drying for five days under vacuum. Upon drying, γ does not change significantly, σ_0 decreases $\sim$20%, and T_0 increases $\sim$50%. Thus small variations of the water content between different samples lead to negligible effects on T_0 as compared to those due to aging.

1. Experimental facts

For the three series of samples the temperature dependence of the conductivity was measured. Depending on the degree of aging, the conductivity could be followed over 2–9 orders of magnitude. The thermal variations of the normalized conductivity $\sigma(T)/\sigma(273)$ are presented in Fig. 8 for samples aged at 100 °C. Similar behaviors are observed for aging at 120 and 140 °C. As can be seen, the relative variation becomes more pronounced with increasing aging times.

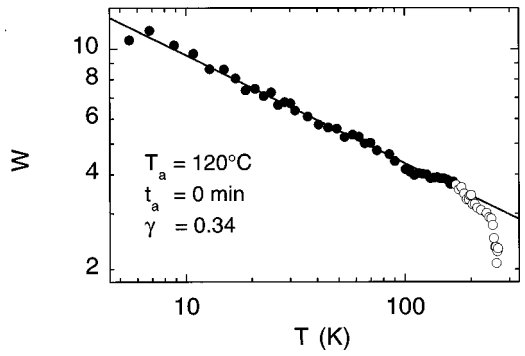

FIG. 9. Determination of the exponent γ by plotting the logarithmic derivative W defined in Eq. (7) as a function of the temperature. γ is obtained as the slope of the straight line.

It appears that for all samples, the temperature dependence of the conductivity is well described by

$$\sigma=\sigma_0 e^{-(T_0/T)^{\gamma}}. \tag{6}$$

The most sensible way to verify Eq. (6) is not a direct fit but a plot of the logarithmic derivative W defined by Eq. (7) as a function of temperature on a double-logarithmic scale:

$$W=\frac{d\ \ln\ \sigma}{d\ \ln\ T}=\gamma\left(\frac{T_0}{T}\right)^{\gamma}. \tag{7}$$

An example is shown in Fig. 9. The straight line corresponds to the behavior given by the Eqs. (6) and (7). The slope gives the value of γ with a high accuracy. γ is scattered around 0.35 without varying systematically with aging time (see Table II). Actually, by using γ as derived from Eq. (7), a good agreement between data and Eq. (6) is observed, except for a slight deviation above 220 K. However, the analysis of the aging effect on conductivity is quite impossible in this framework. It appears that neither γ nor T_0 vary in a monotonic way with aging times, while σ_0 is scattered around an average value. Therefore, in order to go further, we have chosen to set a constant value for γ and to focus on T_0 and σ_0. On the one hand, it would be natural to take $\gamma=0.35$, the experimental mean value. On the other hand, to correlate the effect of aging to an evolution of microscopic parameters requires analyzing the data in the framework of a physical meaningful model. As will be discussed in Sec. V B 2., it appears that the charging-energy-limited tunneling (CELT) and related models[32,33] are actually the most relevant and they lead to $\gamma=\frac{1}{2}$. As one can see in Fig. 8, a rather good agreement of our data with fits using Eq. (6) is obtained when taking $\gamma=\frac{1}{2}$ (solid lines). The values of T_0 obtained from these fits increase with the aging time, the increase being more pronounced for higher aging temperatures (see Table II). T_0 turns out to be the key parameter describing the change of conductivity during aging. A crucial point of our analysis is the fact that the loss of room-temperature conductivity during aging is essentially due to an increase of T_0 and not to a variation of σ_0 (see, in detail, Sec. VI).

2. Charging-energy-limited tunneling between conducting grains

A body of strong arguments suggests a heterogeneous picture for Pani-HCl and aged Pani-HCl. First of all, the structural studies presented in Sec. IV conclude that the aging

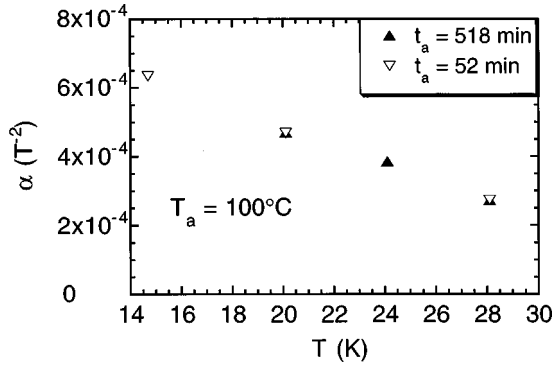

FIG. 10. Temperature dependence of the magnetoresistance coefficient α as defined in Eq. (8) for two samples aged at 100 °C.

process is inhomogeneous, and that the material likely consists of conducting grains separated by amorphous shells of an insulating *F* phase. Second, several transport studies[19] and nuclear relaxation studies[34] have shown the tendency of Pani-HCl to form conducting islands. Finally, let us point out that while the macroscopic conductivity strongly decreases with aging, the microscopic conductivity as probed by spin dynamics studies decreases very slowly.[35,13] Such a behavior is in favor of an inhomogeneous distribution of the disorder in the material. Alternative models predicting the same temperature dependence as that given by Eq. (6), such as quasi-one-dimensional variable range hopping[36] or variable range hopping in the presence of a Coulomb gap at the Fermi level,[37] can be ruled out using the same arguments as in polypyrrole.[15,16] Then remains the variable-range-hopping model of Mott. In this case σ_0 is expected to be very weakly dependent with T_0, as observed experimentally. Let us then examine the magnetoresistance data. Experimentally, the resistivity of Pani-HCl increases with the square of the magnetic field:

$$\frac{\rho-\rho_0}{\rho_0}\approx\ln\left(\frac{\rho}{\rho_0}\right)=\alpha B^2. \tag{8}$$

In Fig. 10, the temperature dependence of α is shown for two samples aged for different times. No influence of aging on the magnetoresistance is detected. In variable-range-hopping models, α is related to the localization length ξ, i.e., to the extension of the states participating to the conduction process. As in these models, disorder is at the origin of localization, ξ in turn should be very sensitive to the degree of aging, which is in contradiction to the results for Pani-HCl.

In summary, models based on homogeneous disorder fail to explain the experimental facts. We therefore propose that the granular structure of Pani-HCl as sketched from x-ray analysis is the key to understand conductivity. We will interpret our results within the model of charging-energy-limited tunneling between conducting grains developed in Ref. 32 and adapted to conducting polymers by Zuppiroli *et al.*[33] In this model, conducting grains are nothing but polaronic clusters. The basic idea of this model is that the hopping frequency between polaronic clusters can be written as the product of two terms: (i) the tunneling probability $\propto\exp[-(2s/a)]$ and (ii) the thermally activated probability to create a pair of charge carriers $\propto\exp[-(E_c/k_BT)]$. Here *s* is the tunneling distance between the grains, and *a* is the decay length of an electronic wave function. The charging energy E_c is the energy required to create a pair of charge carriers by moving a charge from a neutral grain to another. It depends on the grain size *d* and the intergrain distance *s*.

The conductivity is dominated by the process with the maximum hopping frequency. Maximizing the hopping frequency with respect to *d* for a given composition, i.e., under the condition $d/(d+s)=\text{const}$, directly leads to Eq. (6) with $\gamma=\frac{1}{2}$. For T_0, one obtains

$$T_0=\frac{8}{k_B}\frac{e^2}{4\pi\varepsilon_0\varepsilon_r a}\frac{s^2}{d^2}\frac{1}{1/2+s/d}. \tag{9}$$

Deviations of the experimental values of γ from the theoretical value $\gamma=\frac{1}{2}$ may be due to several reasons. Sheng and Klafter considered a distribution of grain sizes. $\gamma=\frac{1}{2}$ results from an interpolation of the results $\gamma=\frac{1}{4}$ and $\frac{1}{2}\leqslant\gamma\leqslant 1$ obtained in the low- and high-temperature limits respectively.[38] Decreasing the grain size and narrowing their distribution function has the effect of extending the validity of the low temperature approximation and thereby of the $\gamma=\frac{1}{4}$ behavior. This could make $\frac{1}{4}\leqslant\gamma\leqslant\frac{1}{2}$ a better overall representation of the numerically calculated temperature dependence of the conductivity resulting from the model of Ref. 38. As the extension of the model by Zuppiroli *et al.* does not explicitly take into account the grain size distribution, it cannot reproduce effects related to its varying width and mean value. The difference in γ between theory and experiment could therefore be attributed to simplifications necessary during the calculation. It must be emphasized that the relative evolution of T_0 is not sensitive to the exact value of γ chosen for the fits. For example, fixing γ to its mean value of $\gamma=0.35$ instead of $\gamma=\frac{1}{2}$ changes the absolute value of T_0, while the relative variations remains almost unaffected.

VI. DISCUSSION

In the framework of the CELT model, the conductivity is related to the granular microstructure. We here propose to model the kinetics of the aging process to account for the changes of the microstructure as observed by x ray. This in turn will permit a quantitative description of the evolution of the conductivity and its temperature dependence.

We suggest the following picture: (i) The material initially consists of conducting grains of ES-I, separated by thin insulating barriers which represent a very small volume fraction; these grains are themselves composed of crystallites surrounded by ''paracrystalline'' and ''amorphous'' ES-I. (ii) The aging process which progressively transforms the material into the insulating *F* phase, is first initiated at the periphery of the grains that is in the most disordered regions. We assume that the *F* phase then expands toward the center of the grains in a diffusionlike manner, as already evidenced for aging in polypyrrole.[16] To further simplify, we consider that the grains are spheres, the average radius of which is *R*. Therefore, the chemically transformed part of grains at time t_a is equal to the overall content of the *F* phase, C_F, in the sample. It can be calculated by solving the diffusion equation for a sphere of radius *R* with an effective diffusion constant *D* (see for example Ref. 39):

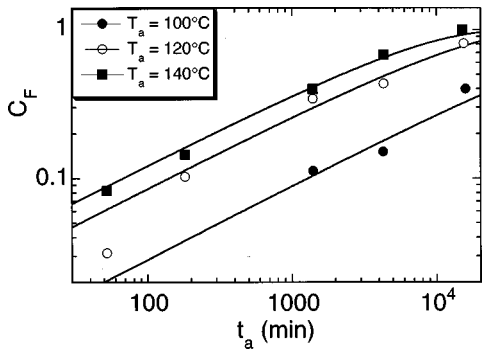

FIG. 11. Concentration of phase F (damaged phase) as a function of the aging time t_a for different aging temperatures. Solid lines represent fits of the data with Eq. (10).

$$C_F(\tau)=1-\frac{6}{\pi^2}\sum_{n=1}^{\infty}\frac{1}{n^2}\,e^{-n^2\pi^2\tau}, \tag{10}$$

with

$$\tau=\frac{Dt_a}{R^2}. \tag{11}$$

Here C_F is a volume fraction, while the data reported in Table II represent weight fractions. Since the difference between these two types of units is inferior to 5%, no correction will be made to Eq. (10).

Figure 11 shows the variation of the F-phase content with t_a for different aging temperatures as well as the fits obtained with Eqs. (10) and (11). One can see the good agreement with the data. The only free parameter is D/R^2 that results in a shift along the time axis. Note that the slope of curves is not adjusted. The conductivity data analyzed below were obtained for samples with $C_F \leqslant 0.67$ and hence $\tau \leqslant 0.066$. For $\tau \ll 1$, Eq. (10) can be approximated by the solution for a semi-infinite medium, i.e., $C_F \propto \sqrt{t_a}$. Under these conditions, the local concentration of the F phase, c_F, mainly changes near the surface of the spheres. The local concentration at a distance x from the surface is then given by

$$c_F(x)=1-\mathrm{erf}\left(\frac{x}{2\sqrt{Dt_a}}\right). \tag{12}$$

As shown in Secs. V B 1 and V B 2, the effects of aging on the conductivity are described by a single parameter, the characteristic temperature T_0. The model of charging-energy-limited tunneling relates T_0 directly to s/d, the ratio of the width of the tunneling barriers to the overall size of the grains. Defining $s/2$, as the depth where the concentration of the F phase is equal to 0.5, we obtain

$$\frac{s}{d}=\frac{\sqrt{\tau}}{1-\sqrt{\tau}}. \tag{13}$$

Knowing D/R^2 from the fit of the C_F variation as a function of aging time with Eqs. (10) and (11), the parameter s/d can be calculated from Eq. (13) and (11). Its values are given in Table II.

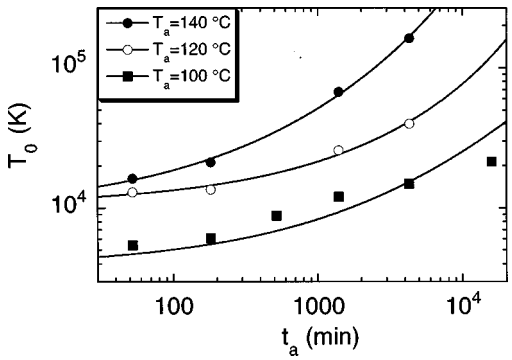

FIG. 12. Variation of the parameter T_0 as a function of the aging time for different aging temperatures. Solid lines are fits of the data with Eq. (9) (see text for details).

Let us now consider the conductivity data and particularly the variation of T_0 with aging time. In the proposed picture, the barrier width s and thereby s/d are roughly proportional to the square root of the aging time. A plot of T_0 versus t_a using logarithmic axes should therefore show a straight line of slope 1. As can be seen in Fig. 12 for short aging times, the variation of T_0 is very weak, becoming more pronounced with progressive aging. To explain these two regimes we assume that, prior to the beginning of the aging process, barriers already exist between the conducting grains. Actually, such barriers are widely invoked to account for the transport properties of pristine highly disordered conducting polymers.[16,19,33] Thus a constant term has to be added in Eq. (13):

$$\frac{s}{d}=\left.\frac{s}{d}\right|_0+\frac{\sqrt{\tau}}{1-\sqrt{\tau}}. \tag{14}$$

Solid lines in Fig. 12 are fits of Eq. (9) with s/d given by Eqs. (14) and (11), and using the previously determined value of D/R^2. The only parameters of the fit, s/d_0, and the prefactor in Eq. (9) are obtained. The prefactor contains the dielectric constant ε_r and the spatial extension of the states participating to the conduction. Since it is essentially the overlap between the valence states of carbon atoms that determines the tunneling probability which is proportional to $\exp[-(2s/a)]$, we use as an estimate $a=1.0$ Å. Under this assumption, we obtained $\varepsilon_r=2.0$, 7.3 and 2.2 for the series aged at $T_a=100$, 120, and 140 °C, respectively. s/d_0 amounts to 0.056, 0.20, and 0.098, respectively. To verify if these values correspond to physically reasonable distances, the absolute grain size $s+d$ has to be known. On the one hand, a lower limit $s+d \geqslant 50$ Å is estimated from the coherence length L_c determined by x ray. On the other hand, the basic assumption of the CELT model is that conductivity is limited by the charging energy, which require $k_BT \leqslant E_c$. As has been shown for polypyrrole for $k_BT \geqslant 1.5.E_c$ significant deviations from Eq. (6) are observed. The fact that for polyaniline Eq. (6) holds well up to 220 K defines an upper limit for the grain size. With $\varepsilon_r=2$ and $s/d=0.1$, we estimate an upper limit for d of 180 Å. Thus a typical value of 100 Å for $s+d$ appears reasonable and consistent with the hypotheses of the model.

According to the proposed picture, the decrease of conductivity during aging is only due to the increase of the

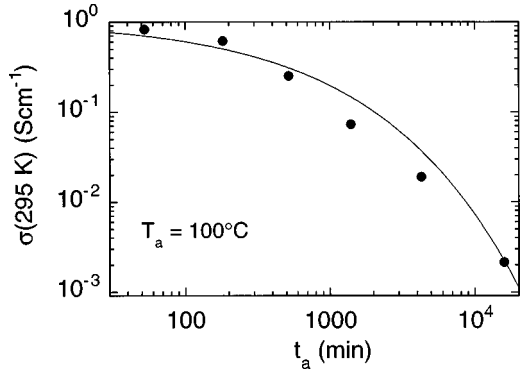

FIG. 13. Room-temperature conductivity $\sigma(295\ \mathrm{K})$ as a function of the aging time t_a at 100 °C. The solid line is obtained from $\sigma(T)=\sigma_0\exp[-(T_0/T)^{1/2}]$, with T_0 given by Eq. (9) and s/d derived from our model (see text).

tunneling length s and of the charging energy E_c. Both are related to the conductivity by the single parameter T_0. A good test for consistency of the model is to check if the increase of T_0 correctly reproduces the decrease of the room-temperature conductivity σ_{RT} during aging at a given temperature. From the evolution of T_0 (the solid line in Fig. 12), the relative change in conductivity has been calculated via $\sigma \propto \exp[-(T_0/T)^{1/2}]$. In Fig. 13, the result is compared to the experimental data for the example $T_a=100\ °\mathrm{C}$. Excellent agreement is found.

VII. CONCLUSION

In the present work, the effects of aging on HCl-doped polyaniline, at a constant temperature in air, were studied by combining thermogravimetric and elemental analyses, x-ray-diffraction studies and conductivity versus temperature studies, as a function of aging time. From x-ray measurements it clearly appears that the aging process is heterogeneous. Besides the crystalline and amorphous emeraldine salt ES-I phases, a phase grows with aging time to the detriment first, of the most disordered part of the material—amorphous ES-I—and, finally, of the ES-I nanocrystallites for long enough times. This phase, which is a damaged phase, is characterized by structural parameters similar to those of dedoped polyaniline, i.e., the emeraldine base. On the other hand, the conductivity data can be interpreted in terms of hopping between conducting grains separated by insulating barriers whatever the aging time is.

We have proposed an overall picture of the aging mechanism, which lies on all the data. In this picture, the conducting grains are initially formed of ES-I crystallites surrounded by shells of ''paracrystalline'' and ''amorphous'' material, and they are progressively transformed into the damaged phase from the periphery toward the center of grains. Assuming that the growth of the damaged phase is driven by a diffusionlike kinetics, we succeeded in accounting quantitatively for the evolution of both the microstructure and the conductivity upon aging. Moreover, from thermogravimetric and elemental analyses, we have demonstrated that contrary to what is generally believed, dedoping due to evolution of gaseous HCl is not the leading mechanism for aging. From a chemical point of view, the formation of the damaged phase appears to mainly consist of oxidation of the polymer backbone due to the presence of oxygen. A concomitant or subsequent chlorination of rings, leading to an effective dedoping of the polymer is strongly suggested.

ACKNOWLEDGMENTS

We are indebted to Y. F. Nicolau, M. Nechtschein, and J. Davenas for fruitful discussions. This work was financially supported by the Agence Rhône Alpes pour la Maîtrise des Matériaux by the project ''Polymères Conducteurs Electroniques.''

*Author to whom correspondence should be addressed.

[1] Y. Wei and K. F. Hsueh, J. Appl. Polym. Sci. **27**, 4351 (1989).
[2] T. Hagiwara, M. Yamura, and K. Iwata, Synth. Met. **25**, 243 (1988).
[3] H. S. O. Chan, P. K. H. Ho, M. M. Tan, B. T. G. Tan, and Y. K. Lim, Synth. Met. **31**, 95 (1989).
[4] Y. Wang and M. F. Rubner, Synth. Met. **47**, 255 (1992).
[5] S. Palaniappan and B. H. Narayana, J. Appl. Polym. Sci. **32**, 2431 (1994).
[6] M. K. Traore, W. T. K. Stevenson, B. J. Mac Cormick, R. C. Dorey, S. Wen, and D. Meyers, Synth. Met. **40**, 137 (1991).
[7] K. G. Neoh, E. T. Kang, and K. L. Tan, J. Macromol. Sci. Pure Appl. Chem. A **29**, 401 (1992).
[8] A. Kobayashi, H. Ishukawa, K. Amano, M. Satoh, and E. Hasegawa, J. Appl. Phys. **74**, 296 (1993).
[9] K. G. Neoh, E. T. Kang, and K. L. Tan, Polym. Degrad. Stab. **43**, 141 (1994).
[10] K. G. Neoh, E. T. Kang, S. H. Khor, and K. L. Tan, Polym. Degrad. Stab. **27**, 107 (1990).
[11] H. S. O. Chan, M. Y. B. Theo, E. Khor, and C. N. Lim, J. Therm. Anal. **35**, 765 (1989).
[12] S. Kim, J. M. Ko, and I. J. Chung, Polym. Adv. Technol. **7**, 599 (1996).
[13] P. Rannou and M. Nechtschein, Synth. Met. **84**, 755 (1997).
[14] B. Sixou, J. P. Travers, and Y. F. Nicolau, Synth. Met. **84**, 703 (1997).
[15] B. Sixou, N. Mermilliod, and J. P. Travers, Europhys. Lett. **30**, 157 (1995).
[16] B. Sixou, N. Mermilliod, and J. P. Travers, Phys. Rev. B **53**, 4509 (1996).
[17] B. Sixou, M. Vautrin, A. J. Attias, and J. P. Travers, Synth. Met. **84**, 835 (1997).
[18] M. Ahlskog, Reghu Menon, A. J. Heeger, T. Noguchi, and T. Ohnishi, Phys. Rev. B **55**, 6777 (1997).
[19] See, for example, E. Zuo, M. Angelopoulos, A. G. MacDiarmid, and A. J. Epstein, Phys. Rev. B **36**, 3475 (1987); H. H. S. Javadi, F. Zuo, K. R. Cromack, M. Angelopoulos, A. G. MacDiarmid, and A. J. Epstein, Synth. Met. **29**, E409 (1989).
[20] A. G. MacDiarmid, J. C. Chiang, A. F. Richter, N. L. D. Somasiri, and A. J. Epstein, *Conducting Polymers: Special Applications* (Reidel, Dordrecht, 1987), p. 105.
[21] P. Beadle, Y. F. Nicolau, E. Banka, P. Rannou, and D. Djurado, Synth. Met. **95**, 29 (1998).
[22] L. B. Valdez, Proc. IRE **42**, 420 (1954).
[23] V. G. Kulkarni, L. D. Campbell, and W. R. Mathew, Synth. Met. **30**, 321 (1989).

[24] A. J. Epstein, Z. Zong, P. K. Gallagher, and A. G. McDiarmid, Synth. Met. **41**, 765 (1991).
[25] E. S. Matveeva, R. Diaz Colleja, and E. Sanchez-Martinez, Synth. Met. **67**, 207 (1994).
[26] E. S. Matveeva, R. Diaz Colleja, and V. P. Parkhutik, Synth. Met. **72**, 105 (1995).
[27] T. Hagirawa, T. Demura, and K. Iwata, Synth. Met. **18**, 317 (1987).
[28] J. P. Pouget, M. E. Jozefowicz, A. J. Epstein, X. Tang, and A. G. MacDiarmid, Macromolecules **24**, 779 (1991).
[29] J. E. Fischer, Q. Zhu, X. Tang, E. M. Scherr, A. G. MacDiarmid, and V. B. Cajipe, Macromolecules **27**, 5094 (1994).
[30] W. Ruland, Acta Crystallogr. **14**, 1180 (1961).
[31] M. Nechtschein, C. Santier, J. P. Travers, J. Chroboczek, A. Alix, and M. Ripert, Synth. Met. **18**, 311 (1987); A. Alix, V. Lemoine, M. Nechtschein, J. P. Travers, and C. Menardo, *ibid.* **29**, E457 (1989).
[32] P. Sheng, B. Abeles, and Y. Arie, Phys. Rev. Lett. **31**, 44 (1973).
[33] L. Zuppiroli, M. N. Bussac, S. Paschen, O. Chauvet, and L. Forro, Phys. Rev. B **50**, 5196 (1994).
[34] P. Y. Mabboux, B. Beau, J. P. Travers, and Y. F. Nicolau, Synth. Met. **84**, 985 (1997).
[35] E. Houzé and M. Nechtschein, Phys. Rev. B **53**, 14 309 (1996).
[36] Z. H. Wang, A. Ray, A. G. MacDiarmid, and A. J. Epstein, Phys. Rev. B **43**, 4373 (1991).
[37] B. I. Shklovskii and A. L. Efros, *Electronic Properties of Doped Semiconductors* (Springer, Berlin, 1984).
[38] P. Sheng and J. Klafter, Phys. Rev. B **27**, 2583 (1983).
[39] J. Crank, *The Mathematics of Diffusion* (Oxford University Press, Oxford, 1957).